

Combining crystal structure prediction and simulated spectroscopy in pursuit of the unknown nitrogen phase ζ crystal structure

Watit Sontising and Gregory J. O. Beran ^{*}

Department of Chemistry, University of California, Riverside, Riverside, California 92521, USA

 (Received 27 March 2020; accepted 18 May 2020; published 4 June 2020)

The structure of nitrogen phase ζ remains unknown decades after it was first observed spectroscopically, despite numerous experimental and theoretical investigations. The present computational study performs crystal structure prediction using *ab initio* random structure searching and density functional theory to identify candidate structures. These candidates are then analyzed for consistency with experiment in terms of their simulated x-ray diffraction patterns and Raman spectra. While none of the structures generated here is a clear match for the phase- ζ experimental data, several of the candidates do exhibit features in common with the experiments and could provide an interesting starting point for future studies. The techniques here also rule out several candidate ζ nitrogen structures that have been identified previously. Finally, one of the structures might be considered a candidate for phase κ , whose structure is also unknown.

DOI: [10.1103/PhysRevMaterials.4.063601](https://doi.org/10.1103/PhysRevMaterials.4.063601)

I. INTRODUCTION

Nitrogen exhibits fascinating behavior in the solid state, with at least 15 experimentally reported phases: α , β , γ , δ , δ_{loc} , ϵ , ζ , ζ' , η , θ , ι , κ , λ , *cg*, *lp/bp*, and *hlp* [1–19]. Most of these phases are molecular and ordered, but some are disordered (β [4], δ [14]), nonmolecular (*cg* [12], η [9,10], *lp/bp* [15,19], *hlp* [18]) and/or amorphous (η). The large number of viable molecular packing motifs stems from the small size of molecular N_2 and its weak, nonpolar intermolecular interactions, which make many packing arrangements and orientations energetically competitive.

Mapping out the high-pressure phase diagram of nitrogen has proved challenging due to the overlapping temperature and pressure regions in which individual phases have been observed. In some cases the observed phases are the thermodynamically stable ones, while in others they are kinetically accessible along certain temperature and pressure pathways through the phase diagram. For example, despite being discovered only very recently, the λ phase coexists with nine other known nitrogen phases [16], and it is believed to be the thermodynamically most stable phase over a significant portion of its temperature and pressure range [16,20].

Solving the crystal structures of several high-pressure phases has also proved difficult experimentally. The λ [16] and ι [17] phases were solved only recently via combination of experiment and crystal structure prediction. The structures of the ζ , κ , and θ phases remain unknown, however. The structure of molecular phase ζ has attracted particular attention, as it marks the “frontier” phase in the transition from molecular to nonmolecular phases at high pressure.

Room-temperature compression of phase ϵ induces the transition to phase ζ at around 60 GPa [21]. At low temperatures, this transition occurs at even lower pressures, around

25 GPa [5,8,22]. This transition was first observed optically via Raman spectroscopy [5,8,21] and later confirmed via x-ray diffraction [13,23,24]. It remains stable until around 115 GPa, after which it converts to the monoclinic κ phase at ambient temperature [13] or to nonmolecular phases at high temperatures [12].

Initial proposals suggested that phase ζ had *R3c* symmetry [5,8], though this subsequently proved inconsistent with low-temperature Raman and infrared data [22]. In 2004, Eremets *et al.* attempted to solve the crystal structure of phase ζ using powder x-ray diffraction [23]. Their proposed orthorhombic crystal structure contained four molecules in a unit cell and adopted one of the *P222*₁, *P2*₁*2*₁*2*, or *P2*₁*2*₁*2*₁ space groups, with *P222*₁ being considered most likely. However, a follow-up study argued against the *P222*₁ space group based on further analysis of Raman and x-ray diffraction data [24]. In 2007, Gregoryanz *et al.* reexamined the crystal structure of phase ζ by using single-crystal x-ray diffraction [13]. They suggested that the orthorhombic unit cell contains eight molecules instead of four and adopts a *Pnma* space group. They remained unable to solve for the atomic positions, however.

Computationally, Hooper *et al.* employed *ab initio* crystal structure prediction to search for the ζ -phase structure [25]. Their genetic algorithm search relaxed and ranked structures using plane-wave density functional theory (DFT) and the Perdew-Burke-Ernzerhof (PBE) functional. They produced two groups of structures based on the space groups reported in the experimental studies above. However, the study proved inconclusive. The lowest-energy structures did not adopt the appropriate space groups or cell types. In the end, they narrowed their list of candidates to the four most promising structures: A1 (*Pbcn*), A2 (*P2*₁*2*₁*2*₁), B1 (*Immm*), and B8 (*Pnma*).

Around the same time, Pickard and Needs employed *ab initio* random structure searching (AIRSS) [26] to study

^{*}gregory.beran@ucr.edu

high-pressure crystal structures of nitrogen [27]. They predicted four low-enthalpy structures at high pressure using PBE calculations [27]. One of these structures, monoclinic $P2_1/c$, was later found to correspond to the experimentally observed λ phase [16]. More recently, DFT-driven AIRSS contributed to solving the structure of ι nitrogen, which contains 48 N_2 molecules per cell [17].

Despite these successes, crystal structure prediction alone is not always sufficient. Inaccuracies in the theoretical models and/or the ambiguity surrounding whether an experimentally observed phase is thermodynamically stable or metastable can mean that the most stable candidate structure(s) will not necessarily correspond to the experimentally observed structure. It becomes valuable, therefore, to consider other “orthogonal” observables that can be used to independently assess the agreement between a candidate structure and experimental observations. At ambient pressure, for example, NMR crystallography seeks crystal structure candidates whose predicted chemical shifts match the experimentally observed spectra [28]. In high-pressure systems such as nitrogen, simulated x-ray diffraction data and Raman spectra (particularly for the lower-frequency lattice modes which are sensitive to crystal packing) can prove insightful when analyzing candidate structures.

For example, Hirata and co-workers helped resolve several controversies surrounding the interpretation of experiments on two difference ice phases through *ab initio* simulation of structures and vibrational spectra [29–31]. We employed structure prediction and Raman techniques in arguing that carbon dioxide phases III and VII are actually the same phase [32], and that argument has received subsequent support from *ab initio* modeling of the phase diagram [33]. In nitrogen, simulated Raman spectra played a role in confirming the ι -phase structure, while we used a combination of AIRSS plus simulated powder x-ray diffraction and Raman spectroscopy to help confirm the structure of λ nitrogen [20].

The present computational study attempts once again to solve the structure of ζ N_2 , this time combining structure prediction and simulated spectroscopy. Structures consistent with experimental constraints were generated randomly via the AIRSS protocol. These structures were then refined with dispersion-corrected DFT. Further comparison of the predicted lattice constants, powder x-ray diffraction patterns, and Raman spectra narrows the list of predicted candidates down to just a handful of plausible structures. Moreover, several ζ nitrogen candidates identified in previous studies can be ruled out based on poor spectroscopic agreement. In the end, none of the candidate structures studied here provides a clear match for the experimental data, but a couple are potentially promising enough to merit further study.

II. METHODS

AIRSS structure generation. With sufficient searching, AIRSS ensures broad, unbiased structure prediction. Unfortunately, the complexity of the search space grows exponentially with the number of degrees of freedom. It is therefore common to constrain the search space using whatever experimental information is available. Discovering the 48-molecule unit cell of ι nitrogen would have been virtually impossible

without experimental constraints on the space group and lattice parameters to help focus the search, for example [17].

The AIRSS search here was focused by restraining the randomly generated structures based on experimentally inferred information about the unit-cell type and volume. Specifically, all recent experimental evidence suggests that ζ nitrogen adopts an orthorhombic unit cell with four [23,24] or, more likely, eight [13] molecules per unit cell. Therefore, the AIRSS search was performed over all 59 orthorhombic space groups and cells containing eight N_2 molecules. After selecting the orthorhombic space group at random, the lattice parameters were randomized subject to the constraint that the unit-cell volume lie within $\pm 40\%$ of the experimentally reported volume of 114.8 \AA^3 ($8.6 \text{ cm}^3/\text{mol}$) at 80 GPa [13]. These constraints considerably narrow the random search space and ideally facilitate the structure prediction. On the other hand, the search will likely fail to find the true structure if the experimentally inferred constraints are incorrect.

Once the cell dimensions and space group were selected, a nitrogen molecule was placed at a randomly selected Wyckoff position associated with that space group. The cell was populated with additional symmetry-equivalent molecules by employing the space-group symmetry operators. This procedure of random molecule placement and symmetry-based replication of the molecules was repeated until the cell contained eight molecules. Crystal packings which resulted in intermolecular N_2 distances of less than 1.65 \AA were discarded [25].

Density functional theory structure optimization and enthalpies. The structures generated by the AIRSS approach were then geometry optimized under 80 GPa of external pressure via periodic plane-wave DFT using the B86bPBE density functional [34,35] and the exchange-hole dipole moment (XDM) dispersion correction [36], as implemented in QUANTUM EXPRESSO version 6.2.1 [37,38]. Note that while the XDM dispersion correction is included, the impacts of the correction are small at the high pressures considered here. The DFT calculations employed an 80-Ry plane-wave cutoff and projector-augmented wave (PAW) potentials for nitrogen atoms that were produced using A. Dal Corso’s Atomic code v6.1. Assessment and convergence testing of the plane-wave cutoff and PAW potentials for solid-state nitrogen phases were performed previously [20].

Structures were initially optimized with a $3 \times 3 \times 3$ Monkhorst-Pack k -point grid. After clustering to remove duplicate structures, the structures were refined further with a $6 \times 6 \times 6$ k -point grid. Larger, anisotropic k -point meshes were tested for selected structures with small individual lattice constants, but the structures and enthalpies did not change appreciably. The use of adaptive grids that target consistent k -point density would be more efficient computationally. Space groups for the optimized structures were determined using FINDSYM version 7 [39,40]. Simulated powder x-ray diffraction spectra were generated for each DFT-optimized structure using Mercury [41] and the same 0.3683 \AA wavelength as the experiments [13]. The rmsd15 metric [42] overlaying clusters of 15 molecules from the crystal was employed for selected structure comparisons.

The enthalpies of the candidate structures were estimated by combining the DFT electronic energy with the

pressure-volume term, $H = E_{\text{elec}} + PV$. Vibrational contributions to the molar volume and enthalpy are neglected here. After identifying candidate structures at 80 GPa, the structures were also optimized at 0, 2, 4, 6, 8, 10, 15, 20, 40, 60, 100, 120, and 150 GPa. The equation of state was then interpolated between these data points via cubic splines.

Simulated Raman spectra. Previous work has found that fragment-based correlated wave-function calculations employing second-order Møller-Plesset perturbation theory (MP2) can predict Raman spectra in good agreement with experiment [20,32]. These calculations are made feasible via the fragment-based hybrid many-body interaction (HMBI) model. HMBI partitions the total energy of the nitrogen crystal into contributions arising from individual molecules (one-body), their pairwise intermolecular interactions (two-body terms), and the remaining non-pairwise-additive many-body contributions. The one-body and shorter-range two-body terms (out to 6 Å) are computed with MP2, while the longer-range pairwise and many-body terms are approximated at a lower level of theory:

$$E_{\text{crystal}}^{\text{HMBI}} = E_{\text{1-body}}^{\text{MP2}} + E_{\text{SR 2-body}}^{\text{MP2}} + E_{\text{LR 2-body}}^{\text{Low}} + E_{\text{many-body}}^{\text{Low}}. \quad (1)$$

Only symmetry-unique monomer and dimer fragments need to be computed in evaluating Eq. (1) [43]. The many-body contributions here are largely modeled with the AMOEBA polarizable force field [44] under periodic boundary conditions. Polarizable force field calculations were conducted using TINKER version 6.3 [45] with existing AMOEBA force field parameters for the N_2 molecule [44].

To simulate Raman spectra, the atomic positions were first relaxed via the MP2/aug-cc-pVDZ + AMOEBA HMBI approximation within fixed DFT unit-cell parameters. Harmonic phonon frequencies were then computed at the zone center ($\mathbf{k} = 0$) by diagonalizing the Hessian matrix computed from the second derivative of Eq. (1) with respect to atomic positions. The one- and two-body fragment contributions to the Hessian were computed analytically using GAUSSIAN 09 [46]. Raman intensities were approximated via finite difference of the polarizability derivatives using only the one- and two-body MP2 terms from Eq. (1) [29]. Neglecting the intermolecular many-body contributions is not expected to have a large impact on the Raman intensities for nonpolar N_2 . This protocol is very similar to ones that proved effective in previous simulated Raman studies of high-pressure nitrogen and carbon dioxide phases [20,32].

Finally, fragment-based calculations were performed to refine the unit-cell volumes of selected crystal structures. These calculations combined complete-basis-set MP2 monomer and dimer fragments with a periodic Hartree-Fock/pob-TZVP basis treatment of the long-range and many-body terms using a protocol described previously [20]. However, the periodic Hartree-Fock calculations with the Gaussian basis set proved difficult to converge above ~ 30 GPa of pressure. Accordingly, data computed at 0, 2, 4, 6, 8, 10, 15, 20, 25, and 30 GPa was fitted to a Murnaghan equation of state,

$$H(V) = H_0 + \frac{B_0 V}{B'_0} \left[\frac{(V_0/V)^{B'_0}}{B'_0 - 1} + 1 \right] - \frac{B_0 V_0}{B'_0 - 1}, \quad (2)$$

where the enthalpy (H_0), volume (V_0), bulk modulus (B_0), and its first pressure derivative (B'_0) at zero pressure are fitting parameters. The limited pressure range potentially limits the reliability of the equation of state at higher pressures.

III. RESULTS AND DISCUSSION

A. Crystal structure prediction

Nearly 1 300 structures with orthorhombic space groups were generated randomly for the AIRSS search. After initial B86bPBE-XDM relaxation at 80 GPa of external pressure with the modest $3 \times 3 \times 3$ k -point grid, about half of the random structures optimized to network covalent and/or polymeric forms. Those structures were discarded from this study due to (1) their significantly higher enthalpies compared to molecular forms at 80 GPa and (2) because all experimental evidence suggests ζ nitrogen is a molecular phase [5,8,13,23,24]. Space-group symmetry was not enforced during the relaxations. Of the 636 remaining molecular structures, 553 relaxed orthorhombic space groups. The other 83 relaxed to monoclinic, triclinic, or tetragonal structures and were discarded. After clustering based on crystal packing similarity, 34 unique molecular crystal structures remained. Each of these 34 structures was generated multiple times during the AIRSS search, and several of them were generated tens of times.

The crystal structures of these 34 candidates were subsequently refined with the denser $6 \times 6 \times 6$ k -point grid. This additional relaxation caused two more pairs of structures to coalesce, leaving 32 unique structures. For convenience, these structures are referred to by number in order of increasing enthalpy, with structure 1 being the most stable. Of these 32 predicted structures, 19 of them lie within 25 kJ/mol of structure 1 at the B86bPBE-XDM level of theory, as shown in the crystal energy landscape plotted in Fig. 1. The remaining structures have even higher relative enthalpies and seem very unlikely to occur at this pressure experimentally. Figure 2 shows selected structures that are discussed in detail below.

From Fig. 1, it is clear that the higher-density structures are generally more stable, as one expects under high external pressures. It is also notable that the DFT-predicted structures underestimate the experimental volume by up to 4% at 80 GPa. This volume underestimation extends across a broad pressure range, as seen from the equations of state plotted in Fig. 3.

However, the volume errors here do not indicate that the predicted structures are inconsistent with experiment. Similar B86bPBE-XDM volume underestimation is seen for the ϵ [see the Supplemental Material (SM), Sec. 4] and λ N_2 phases [20] as well. That study showed how refining the geometries with correlated wave-function methods improved the agreement of the predicted structures with the experimental molar volume, and similar results are obtained here. Figure 3 plots Murnaghan equations of state for three candidate structures (B8, no. 12, no. 19) that were fitted to predictions from the same fragment-based MP2/CBS + pHF approach used in Ref. [20]. Subject to the caveats noted in the Methods section about their accuracy at high pressure, the MP2 results suggest that the candidate structures here do exhibit molar volumes that are consistent with the experimental data for phase ζ .

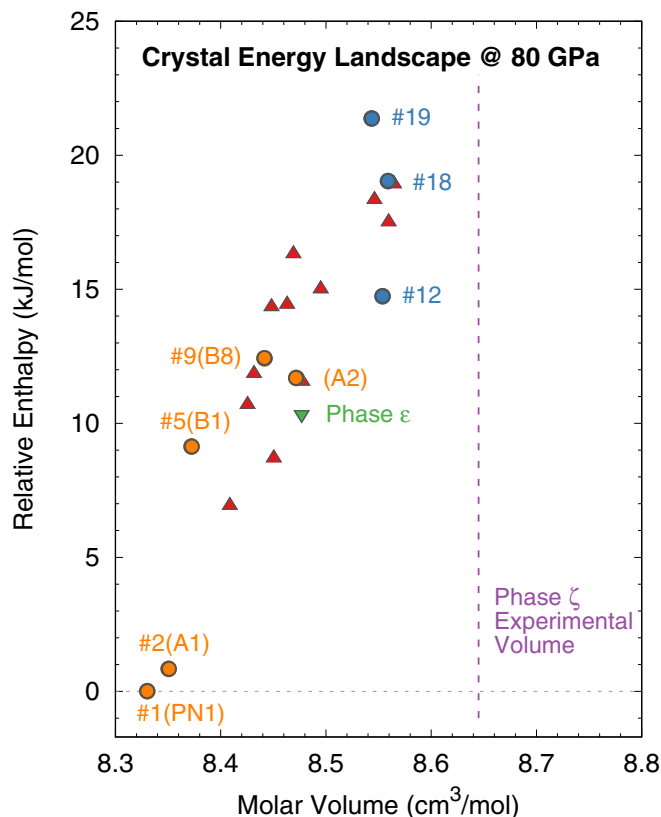


FIG. 1. Predicted crystal energy landscape for orthorhombic molecular N_2 phases at 80 GPa. Structures that have been reported in earlier structure prediction studies are shown in orange, while candidates in blue are new structures discussed in detail below. The enthalpy and volume for the optimized ϵ phase is shown for comparison, along with the reported molar volume of phase ζ .

The 32 unique structures generated here include several structures that were identified in previous crystal structure prediction studies of nitrogen. Structure 1 corresponds to the four-molecule $P4_12_12$ structure found by Pickard and Needs [27]. They also found it to be the most stable structure in this pressure regime. It will be referred to as structure PN1 for the remainder of the present work. Structure 2 matches the four-molecule $Pbcn$ structure of Pickard and Needs [27] and what Hooper *et al.* [25] called structure A1. The search here also found structures corresponding to Hooper *et al.*'s two-molecule $Immm$ B1 (no. 5) and eight-molecule $Pnma$ B8 (no. 9) structures.

The $Z = 8$ search did not discover a supercell corresponding to the A2 structure ($P2_12_12_1$, $Z = 4$) from Hooper *et al.* This does not reflect any fundamental problem of the AIRSS search algorithm: a $Z = 4$ search in the $P2_12_12_1$ space group found A2 readily. Rather, the larger $Z = 8$ cell used here allows the closely related but more stable structure 3 to form instead. When compared against a $Z = 8$ supercell of A2, half of the structure 3 cell is virtually identical to A2, while the other half is related via a twofold screw axis instead of simple translation (see SM Sec. 3 [47]). Because structure 3 lies 5 kJ/mol lower in energy than A2, it was presumably found preferentially in the $Z = 8$ search. Both structures are included in Fig. 1.

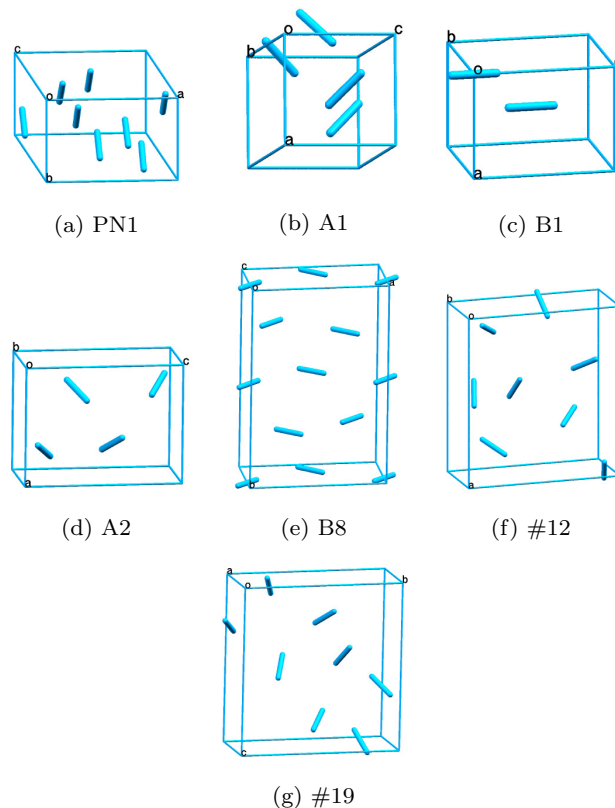


FIG. 2. Selected candidate crystal structures discussed in the text as optimized with DFT at 80 GPa.

From Fig. 1 it is seen that PN1 and A1 are considerably more stable enthalpically than any of the other predicted structures. However, as shown in Table I, none of the aforementioned structures exhibit lattice parameters that are similar to the experimentally reported ones [13]. Looking through the complete set of structures, we find two structures, no. 12 ($P2_12_12_1$) and no. 19 ($P2_12_12$), which have lattice constants in good agreement with the experimentally reported lattice constants. The lattice parameters for structure 19 match experiment to within 0.2 Å, while those for structure 12 match within 0.3 Å. Figure 4 compares the errors between the predicted and experimental lattice constants for several other known N_2 phases computed with the same DFT method. This figure shows that the lattice constant agreement for structures 12 and 19 relative to experiment is consistent with what is found for other high-pressure phases such as ϵ , λ , and ι . The space groups of these two structures also match space groups that were originally suggested for ζ nitrogen [23], even if subsequent work identified an alternative space group [13]. None of the other candidate structures generated in the search appear viable here based on lattice constants (see Sec. II).

While the lattice constant agreement for structures 12 and 19 is encouraging, their enthalpies lie 15 and 21 kJ/mol higher than structure 1, respectively. For crystallization from solution at ambient conditions, the typical energy window for polymorphism is ~ 10 kJ/mol [48], and structures lying more than 10 kJ/mol above the most stable structures are deemed unlikely to crystallize experimentally [49]. The kinetics of high-pressure solid-state phase transitions differ considerably

TABLE I. Comparison of the B86bPBE-XDM lattice constants for several predicted structures compared to the experimentally reported values for ζ nitrogen from Ref. [13]. Only structures 12 and 19 exhibit lattice parameters that are similar to the experimental ones.

| Lattice constants | PN1 <i>P4₁2₁2</i> | A1 <i>Pbcn</i> | B1 <i>Immm</i> | B8 <i>Pnma</i> | 12 <i>P2₁2₁2₁</i> | 18 <i>Pna2₁</i> | 19 <i>P2₁2₁2₁</i> | Expt. (Ref. [13]) |
|-------------------|--|-------------------|-------------------|-------------------|---|-------------------------------|---|----------------------|
| 80 GPa | | | | | | | | |
| <i>a</i> (Å) | 2.690 | 4.241 | 10.450 | 5.294 | 6.176 | 4.287 | 6.298 | 6.507 |
| <i>b</i> (Å) | 5.382 | 2.671 | 3.474 | 7.952 | 2.698 | 5.985 | 2.721 | 2.578 |
| <i>c</i> (Å) | 7.645 | 9.793 | 3.064 | 2.664 | 6.820 | 4.431 | 6.624 | 6.846 |
| 90 GPa | | | | | | | | |
| <i>a</i> (Å) | 2.658 | 4.185 | 10.473 | 5.241 | 6.042 | 4.237 | 6.217 | 6.533 |
| <i>b</i> (Å) | 5.318 | 2.639 | 3.440 | 7.848 | 2.658 | 5.929 | 2.685 | 2.574 |
| <i>c</i> (Å) | 7.556 | 9.696 | 2.972 | 2.630 | 6.808 | 4.370 | 6.558 | 6.844 |

from those of solution-phase crystallizations and can depend on the sample history, but crystal forms lying far outside the 10-kJ/mol window would still seem unlikely to occur experimentally. The stabilities of various candidate structures will be discussed in more detail below.

B. Simulated x-ray diffraction and Raman spectra

Unit-cell representations are not unique, and simple comparisons of lattice parameters may not be sufficient to determine crystal structure similarity. Accordingly, the simulated and experimental powder x-ray diffraction (PXRD) patterns are compared for all candidate structures shown in the crystal

energy landscape (Fig. 1). Selected examples are shown in Fig. 5(a); all others can be found in the SM, Sec. 3 [47]. The simulated diffraction patterns for PN1 and B1 clearly differ significantly from experiment, as do many of the other ones shown in the SM [47]. Structures A1, B8, 12, 18, and 19 exhibit some PXRD features in common with experiment with regard to peak position and, to a lesser extent, peak intensity, although none is a clear match. The PXRD comparison is complicated by the fact that experimentally observed peak intensities can be problematic and sometimes depend on sample history in high-pressure molecular systems such as ζ N₂.

Further insight is gained by simulating Raman spectra for the candidate structures and comparing them against the low-temperature (32 K) experimental spectrum at 30 GPa [8]. Selected species are shown in Fig. 5(b); all others can be found in the SM, Sec. 3 [47]. The DFT underestimation of the molar volumes inhibits intermolecular vibrations and tends to shift

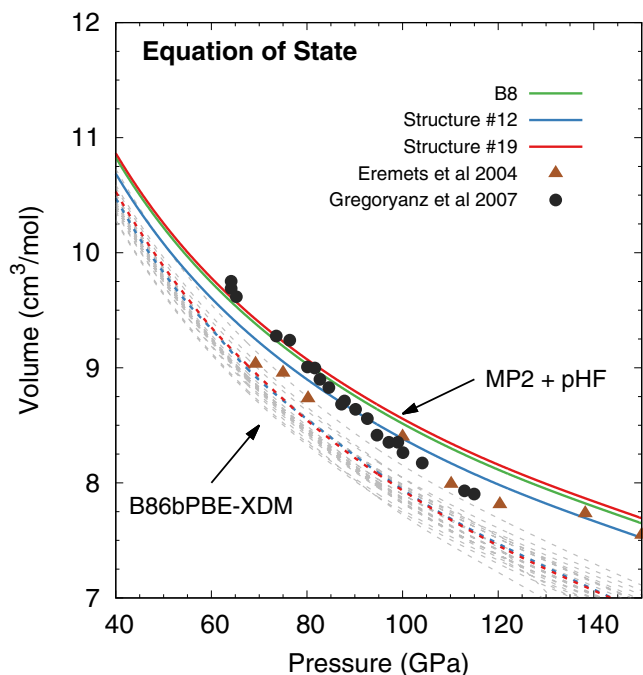


FIG. 3. Comparison of predicted equations of state for all predicted structures against experimental data for nitrogen phase ζ . Dashed lines correspond to the B86bPBE-XDM predicted equations of state for all candidate structures from Fig. 1, with the lines for structures B8, 12, and 19 highlighted in green, blue, and red, respectively. Solid lines show the new equation of state for the selected structures after fragment-based MP2/CBS + pHF refinement.

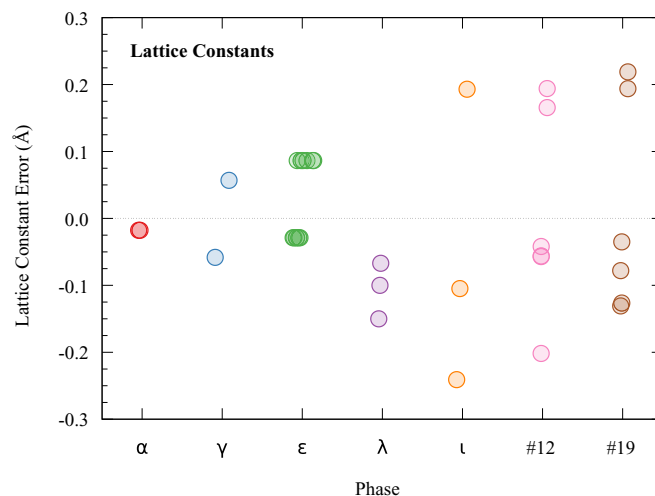


FIG. 4. Comparison between predicted and experimental lattice constants for several known phases of nitrogen and two ζ -phase candidates. The calculations were performed using B86bPBE-XDM with a $6 \times 6 \times 6$ *k*-point grid at the experimental pressure. Where experimental data was available at multiple pressures, errors are shown as computed for each pressure. See the Supplemental Material, Table S1, for details [47].

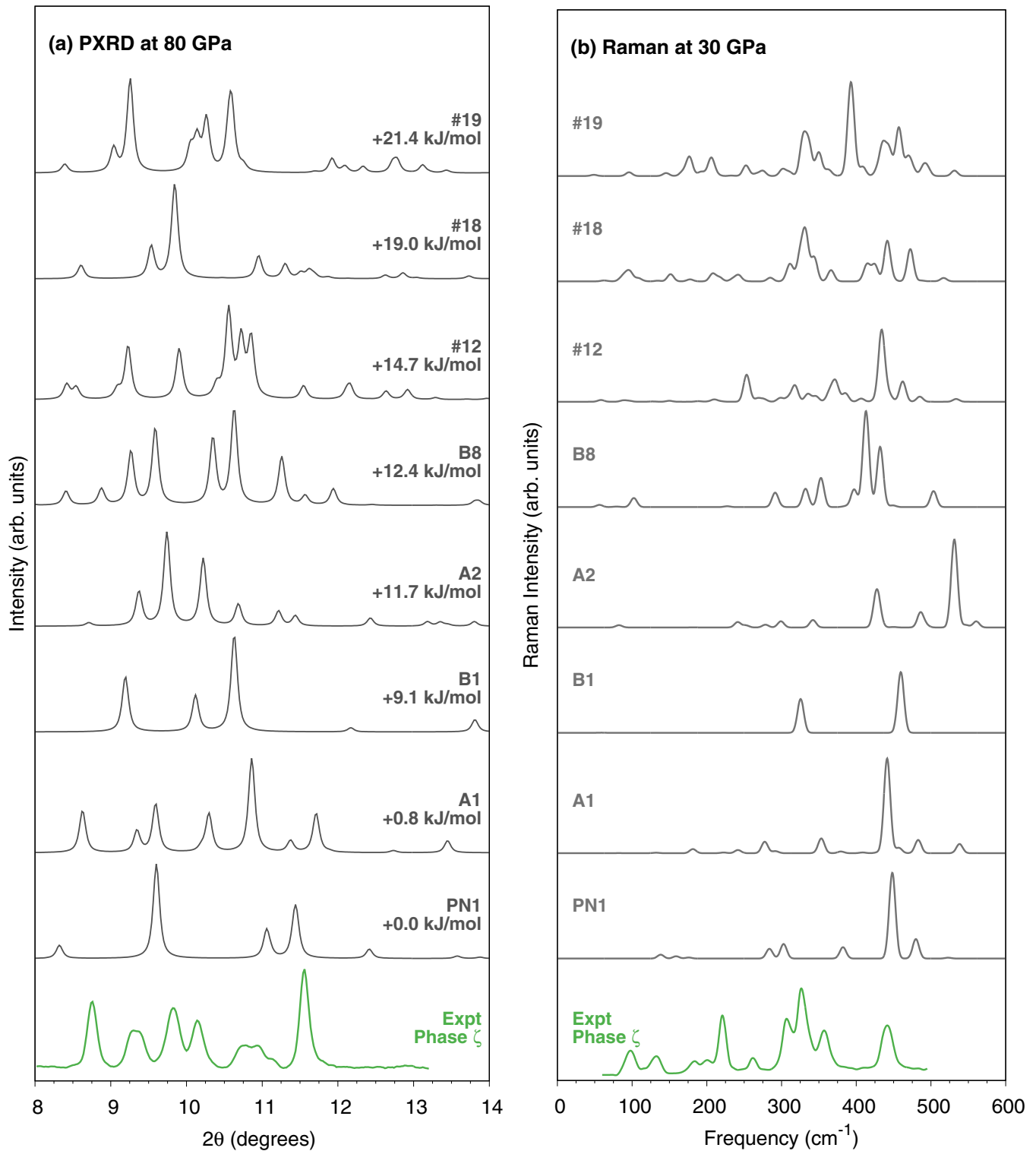


FIG. 5. (a) Simulated powder x-ray diffraction patterns at 80 GPa ($\lambda = 0.3683 \text{ \AA}$) and (b) predicted Raman spectra at 30 GPa for selected candidate structures compared against the experimental data for $\zeta \text{ N}_2$ [8,13]. See Supplemental Material, Sec. 3, for the complete set of simulated spectra [47].

the lattice phonon modes toward higher frequencies. For comparison, consider phase ϵ . Similar to the ζ -phase candidate structures here, the molar volume of phase ϵ is underestimated across the pressure range (SM, Sec. 4 [47]), and this leads to a considerable blue shift in the predicted Raman spectrum.

Testing in smaller unit cells suggests that the small MP2/aug-cc-pVDZ basis set used in computing the frequencies also contributes to the frequencies being overestimated. Using the structure predicted at 20 GPa instead of 30 GPa increases the molar volume and shifts the Raman spectrum toward the red,

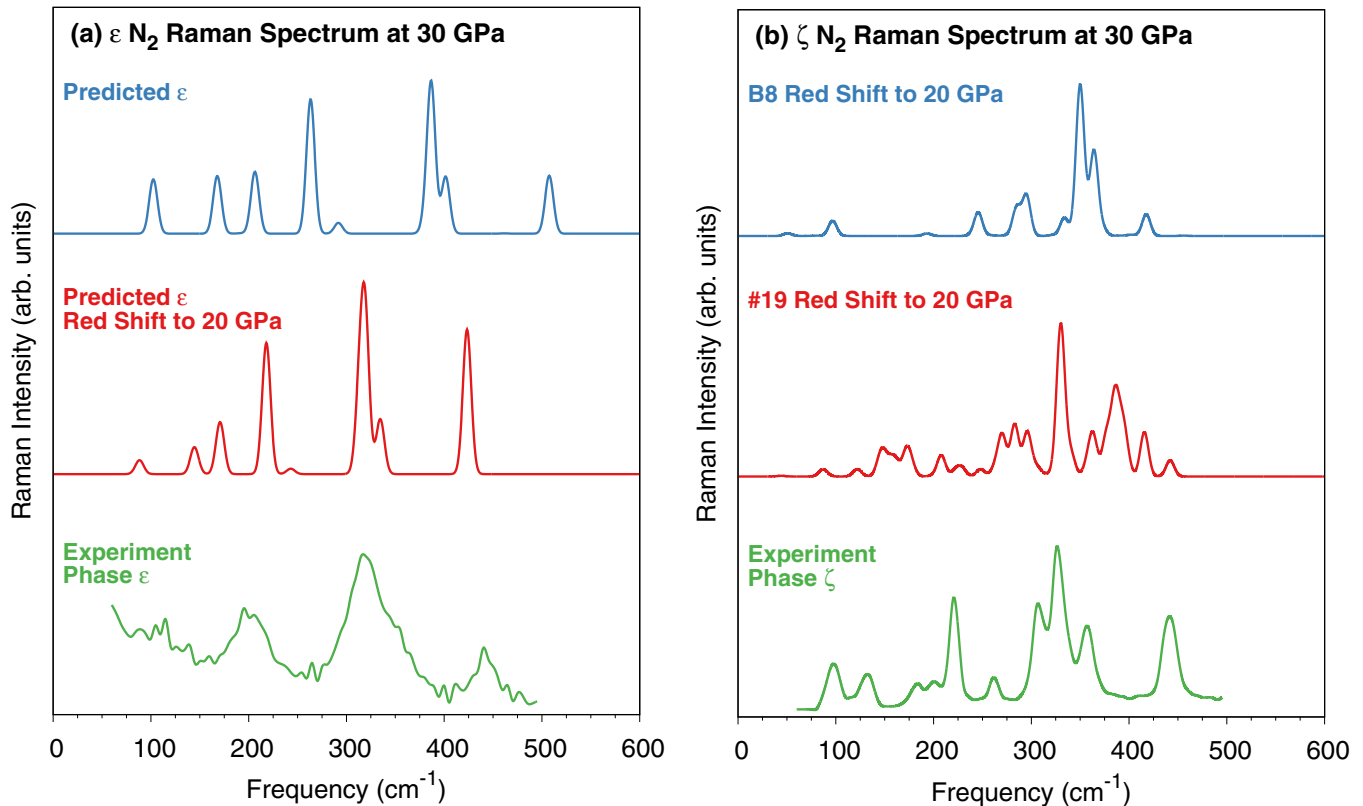


FIG. 6. (a) Reducing the pressure used to compute the predicted spectrum to 20 GPa improves the agreement between theory and experiment considerably for the known ϵ phase. (b) Comparison of the 20-GPa spectra predicted for structures B8 and 19 against the unknown ζ -phase spectrum at 30 GPa. Experimental spectra at 293 K for ϵ and 32 K for ζ taken from Ref. [8].

improving the agreement between the predicted peaks and experimental Raman spectra considerably [Fig. 6(a)].

For the ζ -phase candidates, the vast majority of the predicted structures exhibit Raman spectra that are clearly inconsistent with the experimental spectrum, even if one similarly corrects for the artificial blue shift. Structures such as PN1, A1, B1, and A2 exhibit far fewer Raman-active modes than the experimental spectrum, making them poor candidates for phase ζ . Structure 12 has more Raman-active modes than those others, though the peaks are shifted much too far to the blue and would lack any significant Raman activity below 200 cm^{-1} , even after applying a red shift.

Only three of the structures considered here show plausible resemblance to the experimental Raman spectrum: B8, no. 18, and no. 19. Structure 18 has several peaks in excellent agreement with experiment, such as the trio of peaks just above 300 cm^{-1} and the high-intensity modes at around 450 cm^{-1} [Fig. 5(b)]. On the other hand, it lacks the higher-intensity mode(s) at around 225 cm^{-1} . Red-shifting the structure 18 spectrum using the 20-GPa structure would only reduce agreement further.

The Raman spectra of both B8 and 19 appear shifted too far to the blue, but using the spectrum predicted at 20 GPa instead of 30 GPa improves the agreement with experiment in both cases [Fig. 6(b)]. The shifted B8 spectrum exhibits excellent agreement with the higher-frequency end of the experimental spectrum, particularly above 300 cm^{-1} . On the

other hand, it exhibits little appreciable Raman activity in the $\sim 100\text{--}200\text{ cm}^{-1}$ region, in clear contrast to the experimental spectrum.

The shifted spectrum for structure 19 exhibits some agreement with experiment [Fig. 6(b)], including the pair peaks around 100 cm^{-1} in the experiment that appear near 150 cm^{-1} in the predicted spectrum, plus a high density of peaks in the $\sim 300\text{--}400\text{ cm}^{-1}$ region. However, structure 19 exhibits clear disagreements in other portions of the spectrum, even after the red shift. Interestingly, the $P2_12_12$ structure 19 initially had one imaginary phonon frequency after fragment-based MP2 geometry optimization. Further relaxing the structure along this imaginary coordinate lowers the symmetry to $P2$ and stabilizes the structure by 0.3 kJ/mol (see SM, Sec. 5). This shallow double-well potential could introduce appreciable anharmonicity into the phonon modes that is not accounted for here. While the monoclinic $P2$ symmetry is inconsistent with the experimentally inferred space groups, the barrier is so low that the two structures could readily interconvert (or ground state might even lie above the barrier between the two $P2$ states), meaning that system could adopt the $P2_12_12$ structure on average.

Given the apparent promise of structures 12 (based on lattice parameters) and 19 (lattice constants, space group, PXRD, and Raman), we examine the impact of constraining the lattice constants of those structures to equal the experimental lattice constants reported at 80 GPa and then relaxing

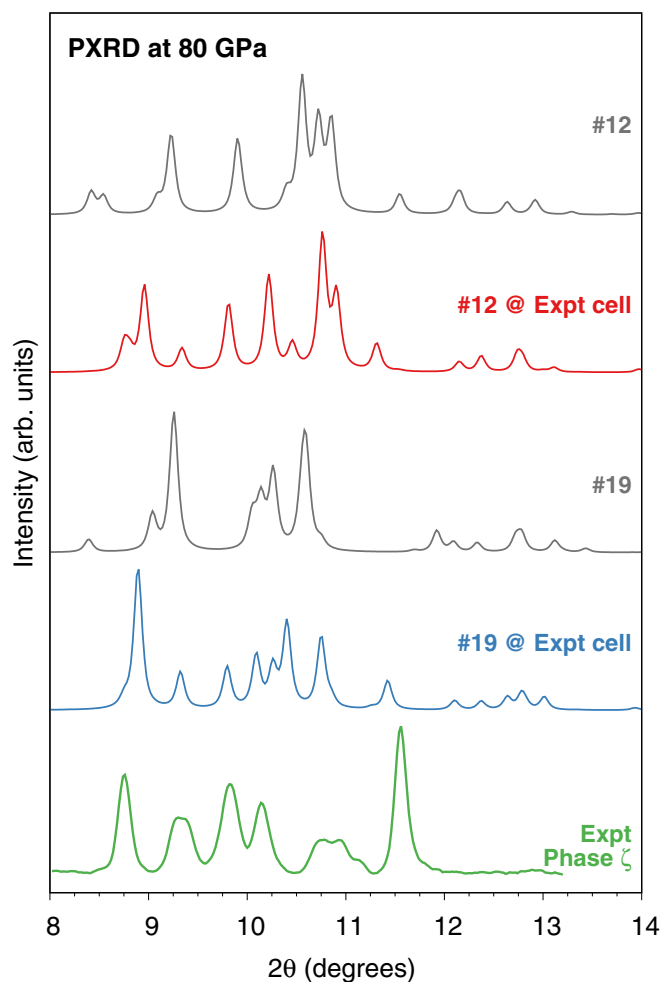


FIG. 7. Comparison of the simulated powder x-ray diffraction patterns of structures 12 and 19 before and after constraining the lattice constants to match the experimentally reported values. All spectra employ a wavelength of $\lambda = 0.3683 \text{ \AA}$.

the atomic positions. Figure 7 shows that constraining the lattice constants in this manner improves the agreement with the experimental peak positions considerably, as one would expect, though the intensity patterns still differ somewhat (especially for the experimental peak near 11.5°). Of the two structures, structure 19, gives the closer match for the experimental PXRD spectrum.

As an aside, we note that the structure of κ nitrogen is also unknown, but preliminary fitting to the experimental diffraction data at 130 GPa suggested a monoclinic cell with lattice parameters $a = 6.92 \text{ \AA}$, $b = 6.20 \text{ \AA}$, $c = 2.29 \text{ \AA}$, and $\beta = 91.8^\circ$ [13]. Because these values are also quite similar to the constants predicted for structures 12 and 19, analogous constrained optimizations were performed on these two structures with the κ lattice parameters at 130 GPa. As described in SM Sec. 6 [47], placing structure 12 in the experimentally reported κ lattice parameters and relaxing it altered the structure only slightly and produced a simulated x-ray diffraction pattern with some similarities to the experimental data. More experimental data would be helpful to assess the structure

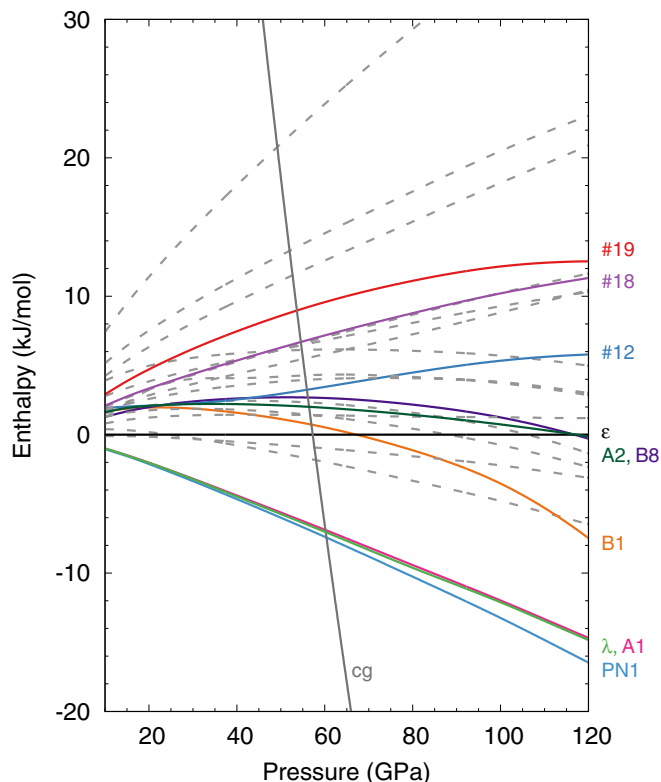


FIG. 8. DFT enthalpies vs pressure for the predicted candidate structures and several experimentally known phases. Colored lines correspond to the key structures; dashed gray lines correspond to other structures from the crystal structure prediction landscape which are not discussed in detail.

further, but structure 12 could be worth pursuing for phase κ as well.

C. Predicted enthalpies

Finally, the pressure-dependent stabilities of these candidate phases relative to several experimentally known phases are considered. Experimentally, the ζ phase is formed by compressing $\epsilon \text{ N}_2$ above ~ 60 GPa at room temperature or at 25 GPa and low temperatures [8,13,21,23,24]. At around 110–130 GPa and 2000 K, ζ nitrogen transforms to the polymeric cubic gauche (*cg*) phase [12,50,51]. The λ phase [16] has proved more difficult to form kinetically, but it overlaps with ϵ , ζ and several other phases and is believed to be more stable than many of those throughout much of the lower-pressure regions of the phase diagram [16,20].

Figure 8 compares the B86bPBE-XDM enthalpies of the candidate structures predicted here and several experimental phases relative to phase ϵ . These enthalpies lack the vibrational free-energy contributions that impact phase stability, but they can still provide helpful insights into the stability regimes of the different phases. Typical vibrational free-energy contributions to polymorph energy differences rarely exceed 2 kJ/mol for organic crystals at ambient conditions, for example [48].

Several features are notable in Fig. 8. First, λ is indeed found to be more stable than ϵ throughout for all pressures

considered here. Moreover, structures A1 and PN1 are also more stable than the ϵ phase over the 10–120 GPa range, and they become increasingly stabilized at higher pressures. So while A1 and PN1 are not experimentally known and are spectroscopically inconsistent with ζ nitrogen, their excellent stability raises the prospect that they might be realized experimentally in the future.

Second, the polymeric cg phase becomes more stable than ϵ at around 60 GPa. This predicted transition pressure is consistent with earlier theoretical studies [27,52–56], but it is inconsistent with the experimental transition happening at around ~ 110 –130 GPa [12,50,51]. This discrepancy likely arises from a mixture of factors:

(1) The entropic effects neglected here stabilize the molecular phases considerably (the entropic difference between molecular and nonmolecular phases can be much larger than between two different molecular phases) [56]. Their inclusion would likely shift the predicted thermodynamic transition point to somewhat higher pressures.

(2) The experimentally observed transition temperature and pressure likely reflect the conditions necessary to overcome the kinetic activation barrier, as evidenced by the fact that the transition pressure varies with the heating method [12,50,51].

(3) Structures 12, 18, and 19 become increasingly less stable relative to ϵ nitrogen as the pressure is increased to 120 GPa (though the slope of the enthalpy curve suggests that structure 19 might begin stabilizing relative to ϵ shortly beyond 120 GPa). If one of those structures did correspond to the ζ phase, there would not be any obvious thermodynamic preference to drive the $\epsilon \rightarrow \zeta$ transition near the 25–60 GPa experimental phase transition pressures (depending on temperature). It seems unlikely that the neglected vibrational free-energy effects would dramatically reduce the stability difference.

(4) B1, A2, and B8 are the only candidates discussed above which become more stable than ϵ at high pressures. For B1, this occurs at around 70 GPa, while for A2 and B8 it occurs just before 120 GPa. These latter two transitions occur well after the regime where cg becomes thermodynamically preferred, though again, that may not be a problem if the experimental transition to the cg phase is kinetically controlled. On the other hand, they also occur well after the experimental $\epsilon \rightarrow \zeta$ transition. However, stabilizing those forms by ~ 2 –3 kJ/mol relative to ϵ would be sufficient to bring the predicted $\epsilon \rightarrow \zeta$ transition back to the appropriate pressure regime. That amount is plausibly within the errors one might expect from the combination of GGA-type DFT functionals and neglecting entropic contributions.

Given all these results, what is the structure of ζ nitrogen? Several of the structures considered here exhibit features that might make them viable candidates. At the same time, each displays some inconsistencies versus experiment that argue against that candidate being the correct structure. PN1 and A1 are clearly the most stable structures identified here (and in previous work), and they have not been ascribed to any experimental phase. However, their spectroscopic properties are clearly inconsistent with experimental observations for the ζ phase. Structures B1 and A2 similarly fail to reproduce the spectroscopic observations. Structure 12 agrees well with

the experimental lattice constants, though its Raman spectrum in particular appears to be a poor match for experiment. It is also considerably less stable than ϵ nitrogen. Structure 18 has some Raman features that are consistent with experiment, but the powder x-ray diffraction spectrum and poor stability argue against it. None of these structures appears to be an appropriate candidate.

Structures B8 and 19 are the best two candidates considered here. Both exhibit plausible simulated x-ray diffraction data and share several features in common with the experimental Raman spectrum (though they each exhibit discrepancies with the Raman spectrum as well). The lattice constants for structure 19 are in good agreement with experiment, and its $P2_12_12$ symmetry matches one of the space groups suggested in earlier work on the ζ phase [23]. On the other hand, the enthalpy of no. 19 is far higher than one would expect for a viable structure. Even if entropy stabilizes structure 19 relative to the ϵ phase, it would likely be too small of a contribution to achieve a phase transition in the relevant pressure regime. Structure B8 is considerably more stable than 19 and even eventually becomes more stable than ϵ at high pressure, though the predicted transition pressure appears to be unrealistically high. Accepting the B8 structure would also require an explanation for the low-frequency Raman bands in the ~ 100 –200 cm^{-1} region that are absent in its simulated spectrum.

IV. CONCLUSIONS

The AIRSS crystal structure prediction approach was employed to search for crystal structures that are consistent with the experimentally reported structural and spectroscopic data for the ζ phase of nitrogen. The structure search did not definitively identify the structure of the ζ phase, but candidates such as PN1, A1, A2, and B1 that have been suggested previously and a number of new structures predicted here can be ruled out based on their spectroscopic properties. The most promising candidates examined here are B8 and no. 19, though neither gives a perfect match for the experimentally observed properties. On the other hand, perhaps these two candidates would provide promising starting points for refining the experimental x-ray diffraction data. That strategy proved helpful in solving the structure of λ nitrogen, for example [16]. The possible connection between structure 12 and the κ phase of nitrogen was also raised, though too little experimental data is available to draw firm conclusions.

If none of these candidates can account for the entire body of experimental evidence, then what is the true ζ structure? After multiple independent structure prediction searches in the literature, it seems unlikely that there exists another low-energy orthorhombic structure with $Z \leq 8$ that has been missed. The possibility of an incorrect interpretation of the experimental diffraction data cannot be ruled out, though that data too has already been examined in a number of studies [13,23,24]. Despite reaching no definitive structural determination for phase ζ , the ability to rule out a number of proposed candidates here demonstrates once again how using the combination of crystal structure prediction and simulated spectroscopy is far more powerful than pure crystal structure prediction alone.

ACKNOWLEDGMENTS

Funding for this work from the National Science Foundation (Grant No. CHE-1665212) and supercomputer time from XSEDE (Grant No. TG-CHE110064) are gratefully acknowledged.

-
- [1] R. W. G. Wyckoff, *Crystal Structures*, 2nd ed. (Interscience Publishers, New York, 1963), Vol. 1, pp. 7–83.
- [2] C. A. Swenson, *J. Chem. Phys.* **23**, 1963 (1955).
- [3] R. L. Mills and A. F. Schuch, *Phys. Rev. Lett.* **23**, 1154 (1969).
- [4] A. F. Schuch and R. L. Mills, *J. Chem. Phys.* **52**, 6000 (1970).
- [5] D. Schiferl, S. Buchsbaum, and R. L. Mills, *J. Phys. Chem.* **89**, 2324 (1985).
- [6] R. L. Mills, B. Olinger, and D. T. Cromer, *J. Chem. Phys.* **84**, 2837 (1986).
- [7] H. Olijnyk, *J. Chem. Phys.* **93**, 8968 (1990).
- [8] R. Bini, L. Ulivi, J. Kreutz, and H. J. Jodl, *J. Chem. Phys.* **112**, 8522 (2000).
- [9] M. I. Eremets, R. J. Hemley, H.-k. Mao, and E. Gregoryanz, *Nature (London)* **411**, 170 (2001).
- [10] E. Gregoryanz, A. F. Goncharov, R. J. Hemley, and H.-k. Mao, *Phys. Rev. B* **64**, 052103 (2001).
- [11] E. Gregoryanz, A. F. Goncharov, R. J. Hemley, H.-k. Mao, M. Somayazulu, and G. Shen, *Phys. Rev. B* **66**, 224108 (2002).
- [12] M. I. Eremets, A. G. Gavriliuk, I. A. Trojan, D. A. Dzivenko, and R. Boehler, *Nat. Mater.* **3**, 558 (2004).
- [13] E. Gregoryanz, A. F. Goncharov, C. Sanloup, M. Somayazulu, H.-k. Mao, and R. J. Hemley, *J. Chem. Phys.* **126**, 184505 (2007).
- [14] G. W. Stinton, I. Loa, L. F. Lundegaard, and M. I. McMahon, *J. Chem. Phys.* **131**, 104511 (2009).
- [15] D. Tomasino, M. Kim, J. Smith, and C.-S. Yoo, *Phys. Rev. Lett.* **113**, 205502 (2014).
- [16] M. Frost, R. T. Howie, P. Dalladay-Simpson, A. F. Goncharov, and E. Gregoryanz, *Phys. Rev. B* **93**, 024113 (2016).
- [17] R. Turnbull, M. Hanfland, J. Binns, M. Martinez-Canales, M. Frost, M. Marqués, R. T. Howie, and E. Gregoryanz, *Nat. Commun.* **9**, 4717 (2018).
- [18] D. Laniel, G. Geneste, G. Weck, M. Mezouar, and P. Loubeyre, *Phys. Rev. Lett.* **122**, 066001 (2019).
- [19] D. Laniel, B. Winkler, T. Fedotenko, A. Pakhomova, S. Chariton, V. Milman, V. Prakapenka, L. Dubrovinsky, and N. Dubrovinskaia, [arXiv:2003.02758](https://arxiv.org/abs/2003.02758) [Phys. Rev. Lett. (to be published)].
- [20] W. Sontising and G. J. O. Beran, *Phys. Rev. Mater.* **3**, 095002 (2019).
- [21] R. Reichlin, D. Schiferl, S. Martin, C. Vanderborgh, and R. L. Mills, *Phys. Rev. Lett.* **55**, 1464 (1985).
- [22] A. F. Goncharov, E. Gregoryanz, H.-K. Mao, and R. J. Hemley, *Low Temp. Phys.* **27**, 866 (2001).
- [23] M. I. Eremets, A. G. Gavriliuk, N. R. Serebryanaya, I. A. Trojan, D. A. Dzivenko, R. Boehler, H. K. Mao, and R. J. Hemley, *J. Chem. Phys.* **121**, 11296 (2004).
- [24] E. Gregoryanz, C. Sanloup, R. Bini, J. Kreutz, H. J. Jodl, M. Somayazulu, H.-K. Mao, and R. J. Hemley, *J. Chem. Phys.* **124**, 116102 (2006).
- [25] J. Hooper, A. G. Hu, F. Zhang, and T. K. Woo, *Phys. Rev. B* **80**, 104117 (2009).
- [26] C. J. Pickard and R. J. Needs, *J. Phys.: Condens. Matter* **23**, 053201 (2011).
- [27] C. J. Pickard and R. J. Needs, *Phys. Rev. Lett.* **102**, 125702 (2009).
- [28] S. E. Ashbrook and D. McKay, *Chem. Commun.* **52**, 7186 (2016).
- [29] X. He, O. Sode, S. S. Xantheas, and S. Hirata, *J. Chem. Phys.* **137**, 204505 (2012).
- [30] K. Gilliard, O. Sode, and S. Hirata, *J. Chem. Phys.* **140**, 174507 (2014).
- [31] S. Hirata, K. Gilliard, X. He, J. Li, and O. Sode, *Acc. Chem. Res.* **47**, 2721 (2014).
- [32] W. Sontising, Y. N. Heit, J. L. McKinley, and G. J. O. Beran, *Chem. Sci.* **8**, 7374 (2017).
- [33] B. H. Cogollo-Olivo, S. Biswas, S. Scandolo, and J. A. Montoya, *Phys. Rev. Lett.* **124**, 095701 (2020).
- [34] A. D. Becke, *J. Chem. Phys.* **38**, 7184 (1986).
- [35] J. P. Perdew, K. Burke, and M. Ernzerhof, *Phys. Rev. Lett.* **77**, 3865 (1996).
- [36] A. Otero-de-la Roza and E. R. Johnson, *J. Chem. Phys.* **136**, 174109 (2012).
- [37] P. Giannozzi, S. Baroni, N. Bonini, M. Calandra, R. Car, C. Cavazzoni, D. Ceresoli, G. L. Chiarotti, M. Cococcioni, I. Dabo, A. Dal Corso, S. de Gironcoli, S. Fabris, G. Fratesi, R. Gebauer, U. Gerstmann, C. Gougoussis, A. Kokalj, M. Lazzeri, L. Martin-Samos *et al.*, *J. Phys.: Condens. Matter* **21**, 395502 (2009).
- [38] P. Giannozzi, O. Andreussi, T. Brumme, O. Bunau, M. Buongiorno Nardelli, M. Calandra, R. Car, C. Cavazzoni, D. Ceresoli, M. Cococcioni, N. Colonna, I. Carnimeo, A. Dal Corso, S. de Gironcoli, P. Delugas, R. A. DiStasio, A. Ferretti, A. Floris, G. Fratesi, G. Fugallo *et al.*, *J. Phys.: Condens. Matter* **29**, 465901 (2017).
- [39] H. T. Stokes and D. M. Hatch, *J. Appl. Crystallogr.* **38**, 237 (2005).
- [40] H. T. Stokes, D. M. Hatch, and B. J. Campbell, FINDSYM, ISOTROPY Software Suite, <http://iso.byu.edu>.
- [41] C. F. Macrae, I. J. Bruno, J. A. Chisholm, P. R. Edgington, P. McCabe, E. Pidcock, L. Rodriguez-Monge, R. Taylor, J. van de Streek, and P. A. Wood, *J. Appl. Crystallogr.* **41**, 455 (2008).
- [42] J. A. Chisholm and W. D. S. Motherwell, *J. Appl. Crystallogr.* **38**, 228 (2005).
- [43] Y. Heit and G. J. O. Beran, *J. Comp. Chem.* **35**, 2205 (2014).
- [44] P. Ren, C. Wu, and J. W. Ponder, *J. Chem. Theory Comput.* **7**, 3143 (2011).
- [45] J. W. Ponder, TINKER v6.3, 2014, <http://dasher.wustl.edu/tinker/>, accessed August 10, 2015.
- [46] M. J. Frisch *et al.*, GAUSSIAN 09, Revision E.01, 2009, Gaussian, Inc., Wallingford, CT.
- [47] See Supplemental Material at <http://link.aps.org/supplemental/10.1103/PhysRevMaterials.4.063601> for additional details of the predicted structures and their spectroscopic properties.

- [48] J. Nyman and G. M. Day, *CrystEngComm* **17**, 5154 (2015).
- [49] J. Bernstein, *Polymorphism in Molecular Crystals* (Clarendon Press, Oxford, 2002), pp. 154–155.
- [50] M. I. Eremets, A. G. Gavriluk, and I. A. Trojan, *Appl. Phys. Lett.* **90**, 171904 (2007).
- [51] M. J. Lipp, J. P. Klepeis, B. J. Baer, H. Cynn, W. J. Evans, V. Iota, and C.-S. Yoo, *Phys. Rev. B* **76**, 014113 (2007).
- [52] A. K. McMahan and R. LeSar, *Phys. Rev. Lett.* **54**, 1929 (1985).
- [53] C. Mailhot, L. H. Yang, and A. K. McMahan, *Phys. Rev. B* **46**, 14419 (1992).
- [54] F. Zahariev, A. Hu, J. Hooper, F. Zhang, and T. Woo, *Phys. Rev. B* **72**, 214108 (2005).
- [55] J. Kotakoski and K. Albe, *Phys. Rev. B* **77**, 144109 (2008).
- [56] A. Erba, L. Maschio, C. Pisani, and S. Casassa, *Phys. Rev. B* **84**, 012101 (2011).